NEGATIVE PRESSURE - FRACTURE STRAIN - TEMPERATURE DIAGRAM

Sakae Saito and Muneaki Shimura
The Research Institute for Iron, Steel, and Other Metals,
Tohoku University, Sendai, Japan

I. INTRODUCTION

The experimental determination of failure maps offers the best approach to workability problems at the present time. Ashby has recently expanded the utilization of such maps in stress-temperature space to demonstrate the relationships between failure modes at various strain rates[1]. The salient feature of his maps is to note that in general we must take cognizance not only of the competition between plasticity and fracture but also the competition between available fracture modes. This raises a third mode of utilization of the failure map viz. the examination of the influence of stress state on the occurrence of a well defined and quantitatively characterized mode of failure[2]. To date, little data is available on this aspect although a valuable progress has been made in the discussion of the influence of hydrostatic (negative) pressure on the strain to failure resulting from voids nucleation and growth[3]. Furthermore, approximate hydrostatic tensile stress states are known to occur, for example, near the root of a notch and may contribute to the brittle fracture of nominally ductile materials.

This presentation illustrates the basic formalism for the portrayal of the failure behaviour of bulk materials under multiaxial stress states.

II. METHOD OF CONSTRUCTION OF THE MAPS

In his pioneering study on the effect of pressure on fracture, Bridgman obtained, for a given longitudinal profile radius of curvature

of the neck of a round bar, an approximate solution for the distribution of stresses and plastic strain across the plane of the neck at the smallest cross section[4]. Direct comparison of the extension of the Bridgman's analysis for the distribution of negative pressure with the results of recent numerical computations[5],[6],[7] demonstrate that his solution is rather good near the neck. Therefore, the neck region of a bar with its distribution of plastic strains and negative pressure along the axis is a convenient plastic flow field for experimental studies of fracture behaviour of the materials[8].

Using pre-notched tensile specimens with semicircular geometries, however, the axial plastic strain increments may no longer be uniform along the plane of the neck, as in predicted by the Bridgman's solution, making that solution no longer valid[9]. The departure from a condition of uniaxial strain in bars with initially machined longitudinal profile is a result of a departure of the machined profile from the natural neck geometry[8]. So, in the first stage of the experiments, a number of natural profiles of necks were carefully measured with the materials used in this work. From such measurements it was determined that the natural neck profile can be expressed with high accuracy by the empirical equation developed by Dondik[10].

Thus, Bridgman-type specimens having natural necking profile after Dondik's equation were machined using a numerically controlled lathe. Those specimens were used in order to investigate the effect of hydrostatic tensile stress on fracture behaviour of the materials.

The experimental results of a steel (S45C) are then expressed in such a way that shown in Fig. 1. The axes are fracture strain, ε_f, temperature, T, and mean maximum hydrostatic tensile component along deformation trajectory, normalized by flow stress, $(\overline{\sigma}_t/Y)$; each datum is plotted as a symbol identifying the mode of failure based on fractographic observation. Open circles indicate that the fracture mechanism was overall fibrous fracture; double circles mean bimodal (fibrous and cleavage) fracture; crossed circles denote overall cleavage fracture. As seen in Fig. 1, fracture behaviour of the material is expressed as a curved surface in three dimensional space (fracture strain-temperature-hydrostatic stress component) and boundaries shown by broken lines are drawn

on the curved surface, separating blocks of data with given modes of failure.

III. FAILURE MAPS FOR COMMERCIAL STRUCTUAL MATERIALS

1. Commercial Structural Steels

The failure maps for S45C-steel, S25C-steel, SM50-steel and high-purity ferritic stainless steel are shown in Fig. 1, Fig. 2, Fig. 3, and Fig. 4, respectively, As seen these diagrams, the higher the hydrostatic tensile stress, the lower the fracture strain. They also show that fracture mode transitions depending on hydrostatic tensile stress and temperature. Under high hydrostatic tensile stress and at low temperature, the steels fail by cleavage. Under the stress states of low triaxiality and at high temperature, they fail in ductile mode. As temperature is decreased and the hydrostatic tensile stress is increased, they exhibit bimodal fracture. In the case of the bimodal fracture, fibrous fracture initiates in the central part of the neck and propagates radially and then a transition from fibrous to cleavage occurs during the propagation as shown in Fig. 5. It is noticeable that two types of transition phenomena from ductile to cleavage are invloved in the process of fracture. The one is as a function of negative pressure and the other is in the propagation of fracture.

Each steel exhibits its own fracture behaviour depending on hydrostatic tensile stress and temperature. For example, the fracture strain of high-purity ferritic stainless steel decreases abruptly as the value of hydrostatic tensile component increases more than those of the carbon steels. The results suggest that special attention should be paid to the conditions of deformation processing of this alloy with coarse-grained structure as used in this work. Producing a fine-grained structure is a most effective means of preventing the occurrence of embrittlement, as already shown in a preceding paper[11].

2. Commercial Structural Nonferreous Alloys

Ti-6Al-4V alloy is a fairly well-investigated titanum alloy

consisting of BCC+HCP phases. Fig. 6 shows the failure map for the Ti-6Al-4V alloy used in this study. It is seen that the higher the hydrostatic tensile stress, the lower the fracture strain, and that the fracture strain decreases slightly as the temperature lowers. Fracture surfaces of all the specimens showed the ductile mode fracture and any transition from ductile to cleavage was not found. From these results, it can be said that this alloy has a good ductility under high hydrostatic tensile stress state and low temperature.

7075 aluminum alloy is a high strength precipitation-hardened alloy and used in the wrought state in the aerospace industry. Fig. 7 shows the failure map for the 7075-T6 aluminum alloy used in this work. As seen in Fig. 7, the higher the hydrostatic tensile stress and lower the temperature, the lower the fracture strain. This alloy dominantly fails intergranularly.

IV. CONCLUDING REMARK

The observation on the fracture behaviour of the Bridgman-type specimens in various materials under the hydrostatic tension can be summarized as "failure map". The map of a given material shows characteristics of fracture of the material in three dimensional space (fracture strain-temperature-hydrostatic tensile component). This presentation illustrates the basic formalism for the portrayal of the failure behaviour of materials. The failure maps may be useful both to compare the fracture behaviour of materials and to extend and compare the failure criteria applicable to bulk materials on a more basic level. There is some hope that the approach might be extend to predict a way in which fracture toughness varies with hydrostatic pressure and temperature.

REFERENCES

[1] Ashby, M. F., Progress in the Development of Fracture-Mechanism Maps, Fracture 1977, vol. 1, LCF4, Waterloo, Canada, (1977), 1.

[2] Embury, J. D. and LeRoy, G. H., Failure Maps Applied to Metal Deformation Processes, ibid. vol. 1, 15.

[3] Rice, J. R. and Tracey, D. M., On the Ductile Enlargement of Voids in Triaxial Stress Fields, J. Mech. Phys. Solids, 17 (1969), 201.

[4] Bridgman, P. W., Studies in Large Plastic Flow and Fracture, (1952), McGraw-Hill Book Co., New York (1952).

[5] Needleman, A., A Numerical Study of Necking in Circular Cylindrical Bars, J. Mech. Phys. Solids, 20 (1972), 111.

[6] Chen, W. H., Necking of a Bar, Int. F. Solids Structures, 7 (1971), 685.

[7] Norris, Jr, D. M. et al, A Computer Simulation of the Tension Test, J. Mech. Phys. Solids, 26 (1978), 1.

[8] Argon, A. S., Im, J. and Needleman, A., Distribution of Plastic Strain and Negative Pressure in Necked Steel and Copper Bars, Met, Trans. 6 (1975), 815.

[9] Clausing, D. P., Stress and Strain Distribution in a Tension Specimen with a Circumferential Notch, Journal of Materials, 4 (1969), 566.

[10] Dondik, I. G., Equation of the Neck Profile of Tensile Specimens, Strength of Materials, (1972), 937.

[11] Saito, S. et al, On the Embrittlement and Toughness of High-Purity Fe-30Cr-2Mo Alloy, ASTM STP706 (1980), 77.

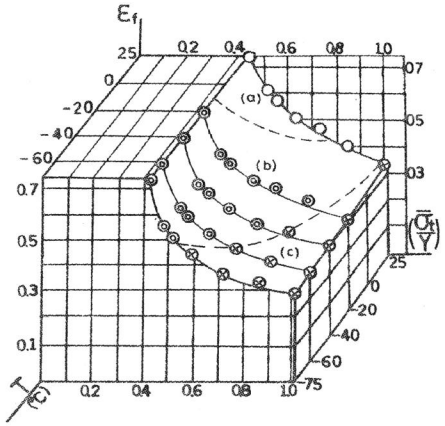

Fig.1 Failure map of S45C-steel : commercial grade 0.45% carbon steel.

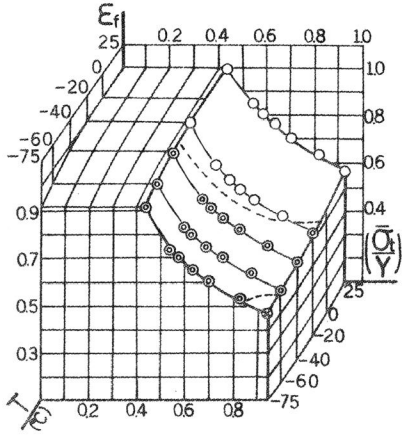

Fig.2 Failure map of S25C-steel : commercial grade 0.25% carbon steel.

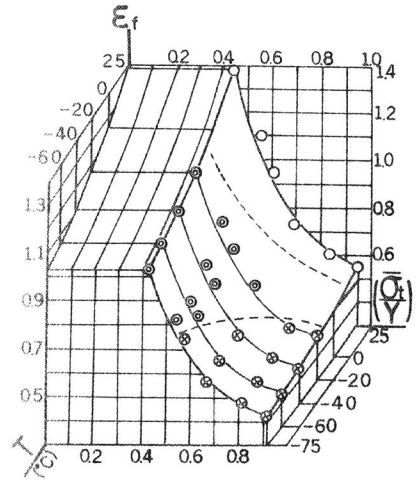

Fig.3 Failure map of SM50-steel : 50kg/mm² class low carbon steel.

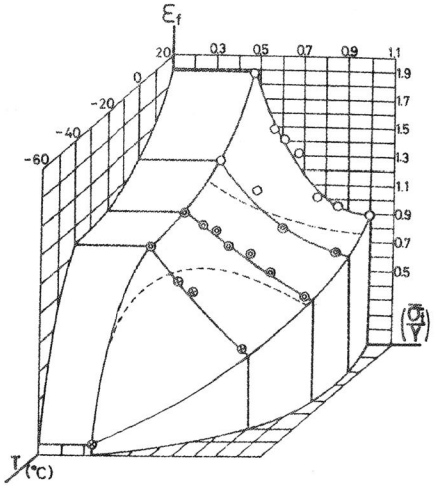

Fig.4 Failure map of high-purity Fe-30Cr-2Mo alloy.

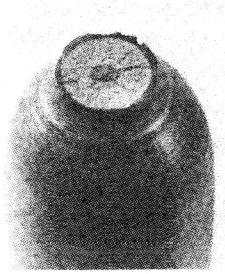

Fig.5 Bimodal fracture surface of Bridgman-type specimen ; dimple fracture mode in the central and cleavage fracture mode in the outer zone.

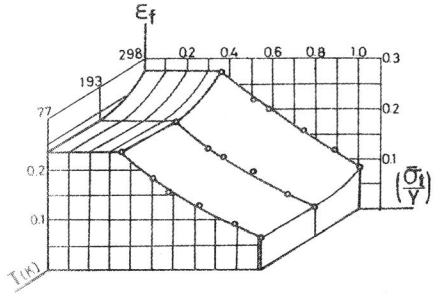

Fig.6 Failure map of Ti-6Al-4V alloy.

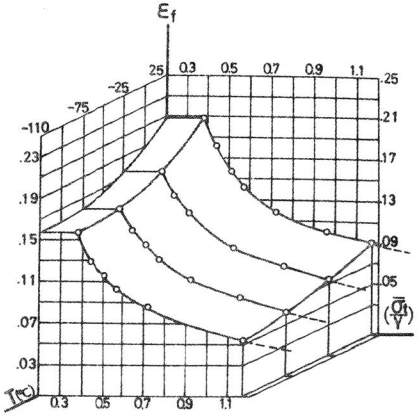

Fig.7 Failure map of 7075-T6 alloy.